

# Fiber amplification of pulse bursts up to $20\ \mu\text{J}$ pulse energy at 1 kHz repetition rate

H. Kalaycioglu,<sup>1,\*</sup> K. Eken,<sup>2</sup> and F. Ö. Ilday<sup>1</sup>

<sup>1</sup>Department of Physics, Bilkent University, Cankaya, Ankara 06800, Turkey

<sup>2</sup>FiberLAST, Ltd., Cankaya, Ankara 06531, Turkey

\*Corresponding author: hamitka@bilkent.edu.tr

Received June 28, 2011; revised August 3, 2011; accepted August 3, 2011;  
posted August 4, 2011 (Doc. ID 150110); published August 23, 2011

We demonstrate burst-mode operation of a polarization-maintaining Yb-doped fiber amplifier. Groups of pulses with a temporal spacing of 10 ns and 1 kHz overall repetition rate are amplified to an average pulse energy of  $\sim 20\ \mu\text{J}$  and total burst energy of 0.25 mJ. The pulses are externally compressed to  $\sim 400$  fs. The amplifier is synchronously pumped–pumped to minimize amplified spontaneous emission between the bursts. We characterize the influence of pump pulse duration, pump-to-signal delay, and signal burst length. © 2011 Optical Society of America  
OCIS codes: 060.2310, 060.2320, 140.3425, 270.2500.

There is much interest in fiber amplification of ultrashort pulses, which offers practical advantages such as low-cost, highly robust, and high-gain amplification. These amplifiers generate pulses that are uniformly spaced in time, typically with repetition rates ranging from tens of kilohertz to several hundred megahertz. However, there are a number of applications for which the ideal pulse pattern is a group of closely and uniformly spaced pulses, i.e., a pulse burst, which is repeated at a low rate (a few kilohertz or lower). An important example concerns photoinjector drive lasers and beam diagnostics lasers in modern accelerator facilities, where the temporal profile of the particle beam is often in the form of a pulse burst [1–3]. In addition, material processing efforts can benefit from a low overall repetition rate for thermal management while making use of the cumulative effect (e.g., through plasma creation) of the momentarily high repetition rate during the burst. Bursts of high-repetition-rate, high-energy pulses are needed to increase the temporal and the spatial resolution in combustion diagnostics [4]. In photoacoustic microscopy, the use of pulse bursts could help increase the signal-to-noise ratio [5]. A burst-mode laser output is well-suited to cavity-enhanced optical parametric amplification [6]. To date, burst-mode laser systems have traditionally been based on solid state lasers, even though a high-repetition-rate burst-mode fiber laser has been used for pulsed laser deposition [7]. Finally, fiber sources can be ideal front ends to solid state amplifiers for applications where the required pulse energy is beyond that which can be provided by a fiber laser.

Here, we demonstrate, for the first time to our knowledge, low-repetition rate, burst-mode operation of a Yb-doped fiber amplifier with a total signal burst energy of  $250\ \mu\text{J}$  at a repetition rate of 1 kHz and average individual pulse energy of  $20\ \mu\text{J}$ . The pulses are externally compressed to 400 fs. One drawback of the high gain in fiber amplifiers is the ease of generation of amplified spontaneous emission (ASE) between pulse bursts at low-repetition rates ( $<10$  kHz), which we circumvent through the use of synchronous pulsed pumping. Experimental characterization of this mode reveals the influence of the main parameters such as signal burst duration, pump pulse duration, and pump-to-signal delay.

The experimental setup (Fig. 1) consists of an all-normal dispersion (ANDi) laser oscillator [8], seeding two stages of core-pumped fiber preamplifiers, and a double-clad (DC) fiber power amplifier as well as synchronized pulse picking and pulse pumping electronics. The fiber oscillator operates at a repetition rate of 100 MHz and outputs 85 mW for a 15 nm wide spectrum, centered at 1037 nm (Fig. 1). The oscillator output is polarized with an inline polarization beam splitter (PBS), followed by polarization-maintaining (PM) components. The seed pulses, with a bandwidth of 16.5 nm, are stretched to 165 ps in a 210 m long PM fiber (with dispersion of  $27\ \text{ps}^2/\text{km}$ ). Next, the signal is amplified in a preamplifier, which is pumped continuously at 976 nm with 450 mW. This is followed by a fiber-integrated acousto-optic modulator (AOM), which impresses the desired pulse burst mode. The bursts are amplified in a second preamplifier, which is pumped by a pulsed pump source with a maximum peak power of 450 mW in synchrony with the signal burst. Because of gain narrowing, the duration of the chirped pulse at the output is measured to be around 120 ps for a signal burst duration of  $1\ \mu\text{s}$ ,  $100\ \mu\text{s}$  pump pulse at a repetition rate of 1 kHz. Part of the output is split with a fiber coupler for monitoring and the remaining power seeds the final amplification stage. The power amplifier is backward-pumped and also

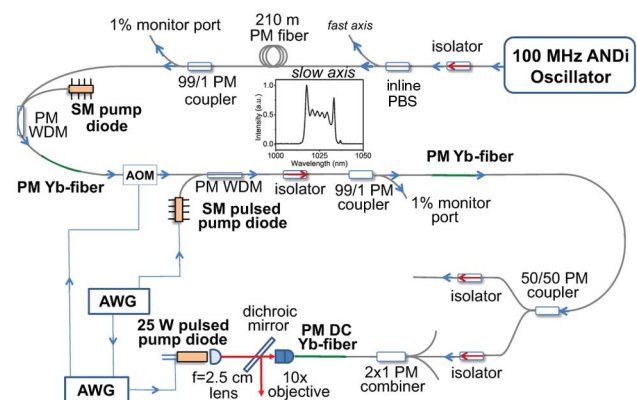


Fig. 1. (Color online) Schematic diagram of the burst-mode amplifier system. SM, single-mode. Inset: spectrum of the seed signal.

operates in a pulsed pumping mode with a maximum peak pump power of 21 W. Two arbitrary waveform generators (AWGs) are used to drive the AOM and the pulsed pump diodes. For the power amplifier, backward pumping through bulk optics and use of a short gain fiber helps minimize the effective nonlinear effects and keep the gain peak around 1030 nm. The gain fiber is a highly doped Yb fiber with a core diameter of 20  $\mu\text{m}$ , a core NA of 0.07, and a cladding diameter of 125  $\mu\text{m}$ . About 70% of the pump power is coupled into the gain fiber with a collimating lens of 2.5 cm focal length and a 10 $\times$  objective.

The burst-mode amplification is investigated in detail at the second preamplifier output at a repetition rate of 1 kHz in order to understand the burst-mode gain dynamics and maximize the energy extraction, while keeping ASE to a tolerable level. Pump-to-signal conversion efficiency, signal gain, and amount of ASE formation are measured as a function of signal burst duration for a pump pulse duration of 100  $\mu\text{s}$  [Fig. 2(a)], and as a function of pump pulse duration for a signal burst duration of 1  $\mu\text{s}$  [Fig. 2(b)]. Pump pulse leads the signal burst with falling edges overlapping such that the two expire simultaneously since any gap between the pump pulse and the signal burst increases ASE generation. ASE amount was estimated by applying, with no signal, a pump pulse of a duration equal to the difference between the corresponding pump pulse and signal burst. It is evident that, for example, although the pump-to-signal conversion efficiency for a 1  $\mu\text{s}$  burst is less than half of that for a 100  $\mu\text{s}$  burst, the signal gain factor is 3.5 times higher. Hence, higher individual pulse energies can be obtained by keeping a high ratio of pump pulse to signal duration, as long as the ASE is kept under control. As a matter of fact, the signal-to-ASE ratio of 10 for the 1  $\mu\text{s}$  burst is much lower than the ratio of 300 obtained for a 50  $\mu\text{s}$  long burst, but it may still be tolerable. Furthermore, the highest pulse amplification with a tolerable amount of ASE peaks for a pump pulse duration of 130  $\mu\text{s}$  [Fig. 2(c)]. For longer

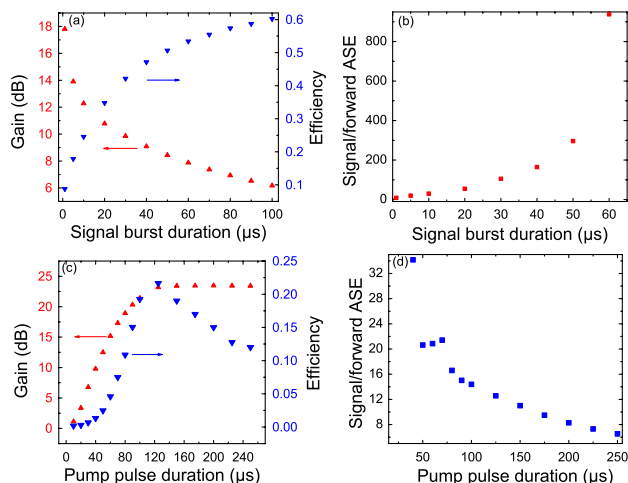


Fig. 2. (Color online) (a) Signal gain (triangles), pump-to-signal conversion efficiency (inverted triangles), and (b) signal-to-ASE ratio versus burst duration for a 100  $\mu\text{s}$  long pump pulse at 1 kHz. (c) Signal gain (triangles), conversion efficiency (inverted triangles), and (d) signal-to-ASE ratio versus pump pulse duration for a 1  $\mu\text{s}$  signal pulse at 1 kHz.

pump pulse durations, the pump-to-signal conversion deteriorates due to unabsorbed pump power, which in turn degrades the signal-to-ASE ratio [Fig. 2(d)].

Following the inclusion of the power amplifier, high-energy operation is characterized. With increasing energies, depletion of the gain during the burst becomes significant, leading to significant variation in energy across the burst. Results of amplification of 1  $\mu\text{s}$  long signal bursts ( $\sim$ 100 pulses per burst) at a repetition rate of 1 kHz are shown in Fig. 3(a). The average pulse energy across the burst is 3.4  $\mu\text{J}$  and the largest pulse energy is 14  $\mu\text{J}$ . This can be partially offset by modulating input burst signal through the AOM such that the net gain times the launched pulse energy is nearly constant. Impressing a fixed ramp on the input burst signal already allows the generation of a significantly more uniform pulse train with the same average pulse energy of 3.4  $\mu\text{J}$ , while the largest energy is 5.5  $\mu\text{J}$  [Fig. 3(b)]. The pump pulse durations for the second preamplifier and the power amplifier are 135 and 130  $\mu\text{s}$ , respectively. It is evident that by impressing a complex variation on the launched burst, one can obtain an arbitrarily uniform amplified pulse train at the cost of decreased efficiency.

Next, we explore limits to individual pulse energy for the burst-mode amplifier. We obtain an average pulse energy of  $\sim$ 20  $\mu\text{J}$  for a burst duration of 150 ns, which contains approximately 13 pulses [Fig. 3(c)]. Identical pumping conditions as in the 1  $\mu\text{s}$  burst case (except slight adjustment of delays) are used and an appropriate ramp gate pulse is applied to the AOM to homogenize the pulse energies within the burst. The highest pulse energy within the burst is 27  $\mu\text{J}$ , with the total burst energy being 250  $\mu\text{J}$  after correction for ASE. This corresponds to a pump-to-signal conversion of 13% with respect to coupled pump power and a net gain of 30 dB for the

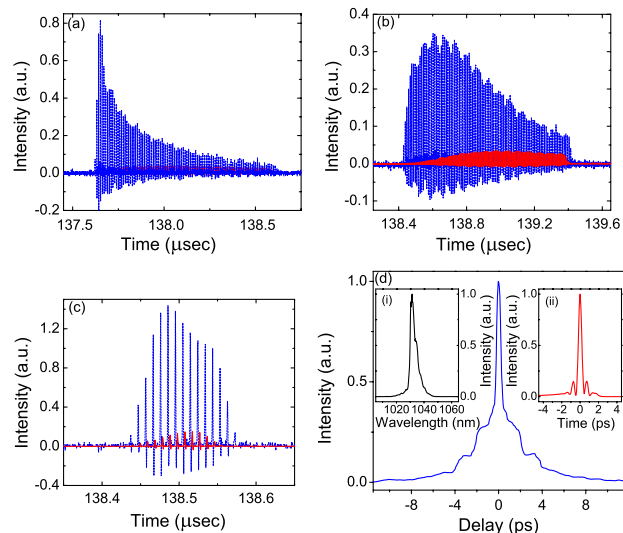


Fig. 3. (Color online) Pulse bursts at the power amplifier input (solid red lines) and output (dashed blue lines) for (a)–(b) different 1  $\mu\text{s}$  signal bursts with average amplified pulse energy of 3.4  $\mu\text{J}$ , and (c) for 150 ns long signal burst, amplified burst energy of 0.25 mJ, highest pulse energy of 27  $\mu\text{J}$ . Seed signals levels are multiplied by a factor of 20 for clarity. (d) Autocorrelation trace for (c). Insets: (i) optical spectrum, (ii) pulse shape obtained from numerical simulations.

power amplifier. The ASE content in the final output is estimated to be about 2.5% via our gain simulation program, and experimentally confirmed to be below 10% as determined by applying the same pump power with no signal. The nonlinear phase shift for the power amplifier at the  $20\ \mu\text{J}$  pulse energy level is estimated to be  $10\pi$  through the numerical simulations based on the method described in [9]. The amplified pulses of a maximum energy of  $20\ \mu\text{J}$  are compressed by an external grating compressor to  $\sim 400$  fs, as inferred from the autocorrelation measurement, assuming a deconvolution factor for a Gaussian pulse [Fig. 3(d)]. Autocorrelation measurement of both the burst mode and uniform repetition rate operation with equivalent pulse energy yields comparable results. The measured duration is consistent with the results of numerical simulations [inset (ii) of Fig. 3(d)], but the pedestals due to uncompensated third-order dispersion (TOD) are experimentally found to be larger than predicted by theory. We attribute this difference to the assumption of a nonlinear chirp-free seed pulse with an idealized Gaussian shape. The amplifier, with its large nonlinear phase shift and TOD mismatch, operates in the nonlinear chirped-pulse amplification regime [10]. Compensation of TOD by self-phase modulation manifests itself in the measured compressed pulse width of 500 fs at the low pulse energy of 3 nJ [11]. High-energy results for the system are shown collectively in Fig. 4. The outcome is parallel with those of the preamplifier in Fig. 2. The nearly equivalent conversion efficiency with burst duration increasing from 1 to  $10\ \mu\text{s}$  is due to the depletion of gain by earlier pulses inside the signal burst.

In conclusion, we report on the burst-mode operation of a PM fiber laser system with 10 ns long pulse-to-pulse spacing within the burst and 1 kHz burst repetition rate. We employ synchronously pulsed pumping to suppress ASE generation between the pulse bursts. The impact of the pump pulse duration, pump-to-signal delay, signal duration on the net gain, and signal-to-ASE ratio were characterized. Signal bursts with total energy of 0.25 mJ and average energy per pulse of  $\sim 20\ \mu\text{J}$  are obtained. We minimize nonlinear effects, including Raman scattering, through the minimization of the effective fiber lengths, such that the pulses are externally compressed to  $\sim 400$  fs. This approach is flexible in that it can be configured to produce virtually any signal burst pattern through adjustment of the oscillator repetition rate, the electronics driving the pump diodes, and the AOM used for gating. Thus, we expect this system, built from off-the-

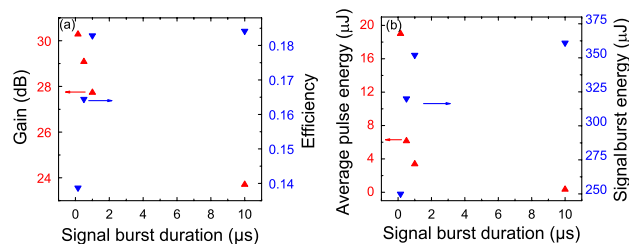


Fig. 4. (Color online) (a) Signal gain (triangles), pump-to-signal conversion efficiency (inverted triangles), (b) average pulse energy (triangles), and total signal burst energy (inverted triangles) versus burst duration at 1 kHz with 2 W average coupled pump power and  $130\ \mu\text{s}$  pump pulse.

shelf components, to find use in various applications requiring bursts of energetic, short pulses.

This work was supported by the European Union (EU) FP7 CROSS TRAP (Grant No. 244068) and SANTEZ Project (No. 00255.STZ.2008-1). We would like to thank Burak Eldeniz for his assistance in data acquisition.

## References

1. H. Braun, R. Corsini, J. Delahaye, A. de Roeck, S. Döbert, A. Ferrari, G. Geschonke, A. Grudiev, C. Hauviller, B. Jeanneret, E. Jensen, T. Lefèvre, Y. Papaphilippou, G. Riddone, L. Rinolfi, W. D. Schlatter, H. Schmickler, D. Schulte, I. Syratchev, M. Taborelli, F. Tecker, R. Tomás, S. Weisz, and W. Wuensch, "CLIC 2008 Parameters," CERN-OPEN-2008-021 (2008).
2. M. Altarelli, in *Magnetism and Synchrotron Radiation New Trends*, E. Beaurepaire, H. Bulou, F. Scheurer, and K. Jean-Paul, eds. (Springer, 2010), pp. 407–409.
3. F. Ö. Ilday, A. Winter, and F. X. Kärtner, *IEICE Trans. Electron.* **E90-C**, 450 (2007).
4. P. Wu, W. R. Lempert, and R. B. Miles, *AIAA J.* **38**, 672 (2000).
5. T. Liu, J. Wang, G. I. Petrov, V. V. Yakovlev, and H. F. Zhang, *Med. Phys.* **37**, 1518 (2010).
6. A. Siddiqui, K.-H. Hong, J. Moses, J. Chen, F. Ö. Ilday, and F. X. Kärtner, *Opt. Lett.* **36**, 1206 (2011).
7. M. Murakami, B. Liu, Z. Hu, Z. Liu, Y. Uehara, and Y. Che, *Appl. Phys. Express* **2**, 042501 (2009).
8. A. Chong, J. Buckley, W. Renninger, and F. W. Wise, *Opt. Express* **14**, 10095 (2006).
9. B. Oktem, C. Ülgüdür, and F. Ö. Ilday, *Nat. Photon.* **4**, 307 (2010).
10. S. Zhou, L. Kuznetsova, A. Chong, and F. W. Wise, *Opt. Express* **13**, 4869 (2005).
11. H. Kalaycioglu, B. Oktem, C. Senel, P. P. Paltani, and F. Ö. Ilday, *Opt. Lett.* **35**, 959 (2010).